

Conformation and Dynamics of Human Urotensin II and Urotensin Related Peptide in Aqueous Solution

Elke Haensele,^a Nawel Mele,^b Marija Miljak,^b Christopher M. Read,^c David C. Whitley,^a Lee Banting,^a Carla Delépée,^d Jana Sopkova-de Oliveira Santos,^d Alban Lepailleur,^d Ronan Bureau,^d Jonathan W. Essex,^b and Timothy Clark.^{e,}*

^aSchool of Pharmacy and Biomedical Sciences, and ^cSchool of Biological Sciences,
University of Portsmouth, Portsmouth PO1 2DT, United Kingdom

^bSchool of Chemistry, University of Southampton, Highfield, Southampton, SO17 1BJ,
United Kingdom

^dNormandie Université, CS 14032 Caen Cedex 5, France, Centre d'Etudes et de Recherche
sur le Médicament de Normandie (CERMN, EA 4258, FR CNRS 3038 INC3M SF 4206
ICORE), UFR des Sciences Pharmaceutiques, Université de Caen Basse-Normandie
(UNICAEN), F-14032 Caen, France

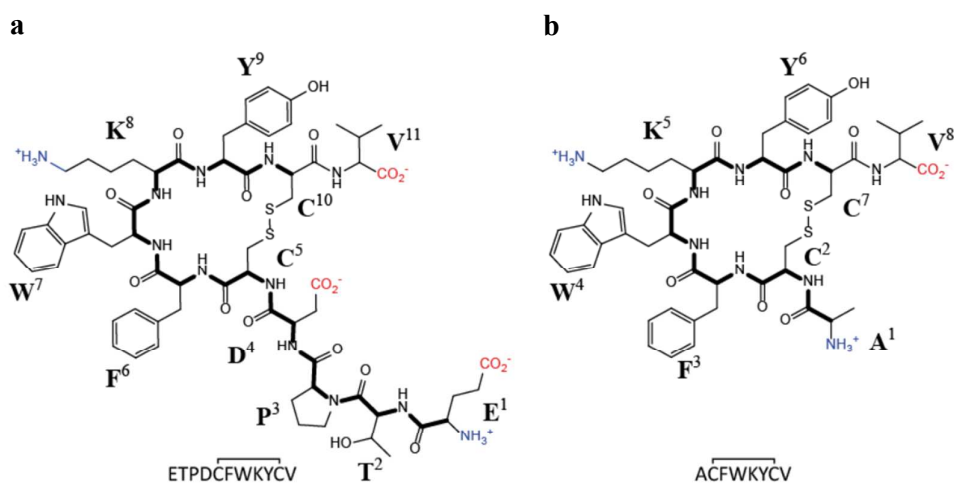
^eComputer-Chemie-Centrum and Interdisciplinary Center for Molecular Materials, Friedrich-
Alexander-Universität Erlangen-Nürnberg, Nögelsbachstraße 25, 91052 Erlangen, Germany

ABSTRACT: Conformation and dynamics of the vasoconstrictive peptides human urotensin-
II (UII) and urotensin related peptide (URP) have been investigated by both unrestrained and

1
2
3 enhanced-sampling molecular-dynamics (MD) simulations and NMR spectroscopy. These
4
5 peptides are natural ligands of the G-protein coupled urotensin II receptor (UTR) and have
6
7 been linked to mammalian pathophysiology. UII and URP cannot be characterized by a single
8
9 structure but exist as an equilibrium of two main classes of ring-conformations, *open* and
10
11 *folded*, with rapidly interchanging subtypes . The *open* states are characterized by turns of
12
13 various types centered at K⁸Y⁹ or F⁶W⁷ predominantly with no or only sparsely populated
14
15 transannular hydrogen bonds. The *folded* conformations show multiple turns stabilized by
16
17 highly populated transannular hydrogen bonds comprising centers F⁶W⁷K⁸ or W⁷K⁸Y⁹. Some
18
19 of these conformations have not been characterized previously. The equilibrium populations
20
21 that are experimentally difficult to access were estimated by replica-exchange MD
22
23 simulations and validated by comparison of experimental NMR data with chemical shifts
24
25 calculated with density-functional theory. UII exhibits approximately 72% *open* : 28% *folded*
26
27 conformations in aqueous solution. URP shows very similar ring conformations as UII but
28
29 differs in an *open:folded* equilibrium shifted further towards *open* conformations (86:14)
30
31 possibly arising from the absence of folded N-terminal tail - ring interaction. The results
32
33 suggest that the different biological effects of UII and URP are not caused by differences in
34
35 ring-conformations but rather by different interactions with UTR.
36
37
38
39
40
41
42
43
44
45
46
47
48
49
50
51
52
53
54
55
56
57
58
59
60

INTRODUCTION

The neuropeptide urotensin-II (UII) was originally found in the urophysis of teleost fishes.¹ A human homolog² of the orphan receptor GPR14³ (a G-protein coupled receptor (GPCR) that is very similar to the somatostatin receptor first isolated from rats) was identified in 1999.⁴⁻⁶ UII is the natural ligand of this receptor, now called the urotensin II receptor (UTS2R, UTR). All vertebrate isoforms of UII show a highly conserved C-terminal sequence: a cyclic 6-residue moiety (CFWKYVC) closed by a disulfide bridge and flanked by valine as extra-annular residue (Scheme 1).⁷ The length of the N-terminus of human UII is four residues but this is species variable, so that the total peptide length ranges from 11 residues for human UII up to 17 for hamster UII.⁷⁻¹⁰ Urotensin related peptide (URP) is a paralog of UII.¹¹ It has the same C-terminal cyclic moiety as UII but the extra-annular N-terminus of UII is replaced by a single alanine at position 1 in URP (Scheme 1).¹² The 6-membered ring closed by a disulfide-bridge is a common motif with other hormone peptides, such as Arg⁸-vasopressin and Leu⁸-oxytocin. UII is the most potent vasoconstrictive natural peptide known² and both UII and URP are thought to be involved in important physiological processes such as cardiovascular regulation, endocrine and behavioral effects.^{7, 8, 11, 13}



Scheme 1. a) Human Urotensin-II (UII) and **b)** Urotensin Related Peptide (URP)

1
2
3 Consequently, they are linked to a multitude of pathophysiological processes such as
4
5 atherosclerosis, heart failure, and many more.^{7, 8, 11, 13, 14}
6
7

8 Although UII and URP show similar potency at the UTR^{12, 15, 16} and apparently have
9
10 overlapping binding sites,¹⁷ their signaling outcomes may, nevertheless, differ.¹³ UII can
11
12 behave as an almost irreversible UTR agonist, and the two peptides can affect astrocyte
13
14 activity differently.^{18, 19} The effects of UII or URP are often not conserved across species^{11, 20}
15
16 and may even be opposite (vasoconstrictive and vasodilative) within the same species.²¹ In
17
18 summary, the urotensinergic system is far from being well understood. Multiallosteric
19
20 interactions of receptor and ligands or biased agonism that ultimately trigger different
21
22 functions have been hypothesized.²²
23
24

25
26 Biological activity studies have shown that the ring sequence UII₍₄₋₁₁₎ is necessary to retain
27
28 full agonistic potency^{16, 23} and that the motif is essential for receptor activation.^{23, 24} An intact
29
30 bridge also seems essential,^{16, 25, 26} but need not be a disulfide.²⁵ However, recently, the first
31
32 acyclic peptide agonist for UTR has been described, a UII-analog that still suggests WKY to
33
34 be the receptor-activating motif.²⁷ Nuclear magnetic resonance (NMR) studies in water^{24, 28}
35
36 and dimethyl sulfoxide,²⁹ supported by circular dichroism (CD) spectroscopy,²⁸ have been
37
38 interpreted to indicate an unstructured form for human UII with no classical turns or
39
40 intramolecular hydrogen bonds. However, Lescot et al.³⁰ inferred, from NMR studies, a
41
42 widened 7,8,9 γ -turn and a 8,9,10 γ -turn with close $W^7O-Y^9H^N$ and $K^8O-C^{10}H^N$ distances for
43
44 the human UII conformation in water, thus localizing a turn center in the ring at residues K^8
45
46 and Y^9 . All NMR investigations show the N-terminal tail to be more flexible than the ring.
47
48 URP has been suggested from the NMR experiments by Chatenet et al.¹⁵ to have an inverse
49
50 4,5,6 γ -turn centered at K^5 in water with the intramolecular hydrogen bond $W^4O-Y^6H^N$. NMR
51
52 experiments by Brancacchio et al.³¹, however, suggest structural flexibility in aqueous
53
54 solution and a high similarity of URP and UII ring-conformations. Carotenuto et al.²⁸ made
55
56
57
58
59
60

1
2
3 NMR studies of UII and the smaller URP-like version, UII₍₄₋₁₁₎, in sodium dodecyl sulfate
4 (SDS) micelles mimicking a cell-surface environment. They found two slowly exchanging
5 states: one specified as β -hairpin with a β -turn type II' centered at W⁷ and K⁸, and another
6 weakly populated, apparently, with a more flexible and random structure. The highly
7 structured state was suggested to be the active conformation in the receptor-binding pocket.
8 Analogous experiments for URP in SDS micelles suggested a very similar structure.³¹
9
10
11
12
13
14
15

16 We now report unrestrained molecular dynamics (MD) simulations of human UII and URP
17 with the Amber ff99sb force field on extended time-scales (see Table S1 and Figures S1-S6 of
18 the Supporting Information, SI). These simulations are designed to investigate the
19 conformational space of the peptides as completely as possible. To rule out small force-field
20 artefacts that might become important for such small peptides, we have also performed
21 additional unrestrained microsecond-scale MD simulations with the CHARMM c36b2 force
22 field. These simulations revealed no significant difference between the conformations
23 obtained with the two force fields, so that we concentrate on the AMBER results, which are
24 more extensive. Replica-exchange molecular dynamics (REMD) simulations have been used
25 to improve the conformational sampling and to obtain thermodynamic information. The
26 results are compared with NMR-spectroscopic experiments and a statistical model of the
27 conformational equilibrium in aqueous solution is given.
28
29
30
31
32
33
34
35
36
37
38
39
40
41
42
43
44

45 METHODS

46
47 **Molecular dynamics simulations.** MD simulations of the peptides UII and URP were
48 performed with Amber 10,^{32, 33} Amber 14 CUDA,³⁴⁻³⁷ and CHARMM c36b2.³⁸ Amber
49 calculations used the ff99SB force field.³⁹ Comparison simulations with CHARMM
50 parameter set 36³⁸ were used to rule out force-field artefacts. REMD simulations were
51 performed with Amber. All simulations were carried out with unrestrained distances and
52 explicit water solvation. Further simulation details are given in the SI (pp S2-S7).
53
54
55
56
57
58
59
60

1
2
3 **Conformational analysis.** Conformational clustering of the backbone dihedrals (*overall*
4 states) was performed with DASH.^{40, 41} Additional sub-clustering of the ring and tail
5 conformations led to a classification of UII and URP conformations in terms of distinct *ring-*
6 *state types*. As representatives, the overall conformations of highest similarity to each *ring-*
7 *state type* were chosen, equivalent to cluster centers (Table S2). Hydrogen-bond populations
8 and secondary structure motifs of characteristic conformations were calculated from
9 corresponding sections of the MD trajectories using AmberTools with default settings.^{33, 34, 42}
10 Consistency of type assignments of states from different simulations was ensured by
11 comparing the circular similarities of ring torsions, turn propensities and C ^{α} alignments.
12 Further details are given in the SI (p S8).
13
14
15
16
17
18
19
20
21
22
23

24 **Principal component analysis.** A possible correlation of ring and tail motions was
25 analyzed with principal component analysis (PCA) implemented in DASH.⁴¹ Torsion weights
26 were calculated from the coefficients of the relevant principal components (PCs). The number
27 of significant PCs was determined by Kaiser's eigenvalue-one test.⁴³ PC clustering was
28 visualized *via* 3D-scatter plots of the three most significant principal components color-coded
29 according to the assigned DASH states in SAR-caddle.⁴⁴ Further details are given in the SI (p
30 S2-S13).
31
32
33
34
35
36
37
38
39

40 **NMR.** NMR spectra were recorded for human U-II and URP at pH 3.0/3.5 and pH 6.0 in
41 H₂O and D₂O on a Varian Inova 600 MHz spectrometer. Proton resonance assignments were
42 achieved using 2D ¹H-¹H total chemical shift correlation spectroscopy (TOCSY),⁴⁵ and ¹H-¹H
43 nuclear Overhauser effect spectroscopy (NOESY) NMR spectra.⁴⁶ Resonance assignments of
44 carbon and nitrogen at natural abundance were achieved through standard ¹³C-¹H gradient
45 heteronuclear single quantum coherence (gHSQC) and ¹⁵N-¹H gHSQC experiments.⁴⁷⁻⁴⁹
46
47
48
49
50
51
52
53
54
55
56
57
58
59
60
Details of sample preparation and NMR experiments are given in the SI (pp S14-S18).

56 **Density-functional theory (DFT) calculations on representative conformations.** The
57 geometries of representative conformations for UII and URP derived from the DASH analysis
58
59
60

1
2
3 were first optimized at the B3LYP⁵⁰⁻⁵³/6-31G(d)⁵⁴⁻⁵⁸ level with Gaussian 09, Revision C.01.⁵⁹
4
5 Water solvation was simulated with the default Polarizable Continuum Model (PCM) using
6
7 the integral equation formalism variant (IEFPCM).⁶⁰ The DFT-optimized structures were
8
9 then used to calculate the magnetic shielding tensors in solution at the same level of theory
10
11 and converted to ¹H, ¹³C, and ¹⁵N chemical shifts using regression formulae based on standard
12
13 sets of chemical shifts and calculated values. The regression formulae and calculated chemical
14
15 shifts are given in the SI (pp S19-S23, Figure S7, Tables S9-S11).
16
17

18 **Equilibrium models and experimental evaluation.** Free energies and relative populations
19
20 (equilibrium models) for the representative conformations of UII and URP were calculated
21
22 from extended REMD simulations. For each peptide, three simulations of 500 ns were
23
24 performed starting from different initial conformations (UII: *omega-I_{open}*, *folded-I*, *lasso*;
25
26 URP: *omega-I_{open}*, *omega-II*, *lasso*). ¹H chemical shifts for the equilibria were calculated *via*
27
28 linear combination of the calculated shifts for the representative conformations according to
29
30 the populations suggested by REMD. The calculated shifts of representatives and
31
32 conformational equilibria were then compared by linear regression with our experimental data
33
34 for non-exchangeable ¹H chemical shifts of UII and URP in aqueous solution at pH 6.0 and
35
36 pH 3.5, respectively.
37
38
39

40 We have recently published details of chemical-shift comparisons for the closely related
41
42 vasopressin and have suggested statistical metrics for judging whether conformational
43
44 equilibria suggested by simulations are consistent with experiment.⁶¹ Here, we used REMD to
45
46 determine equilibrium populations, rather than the metadynamics. This substitution is tested
47
48 here.
49
50

51 Further details are given in the SI (pp S24-S28, Figures S8-S9, Table S13-S15).
52
53
54

55 RESULTS AND DISCUSSION

56 Conformations of Urotensin-II.

57
58
59
60

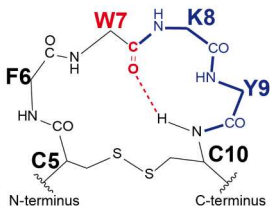
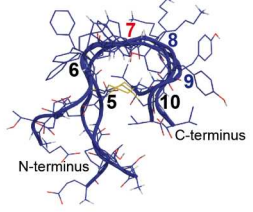
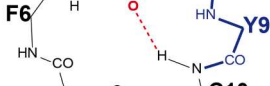
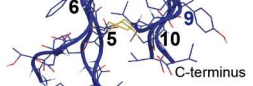
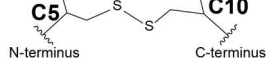

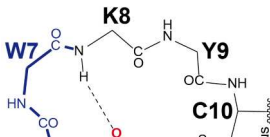
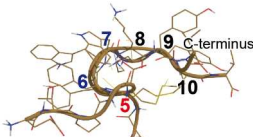
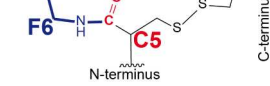
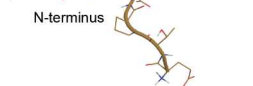
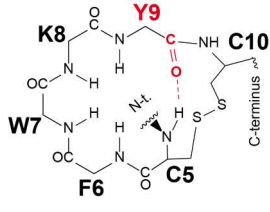
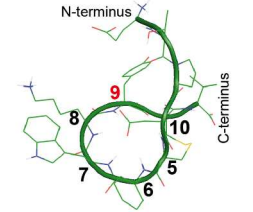
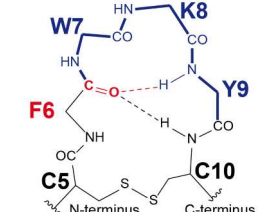
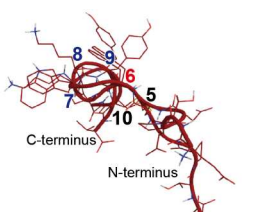
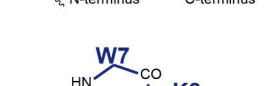

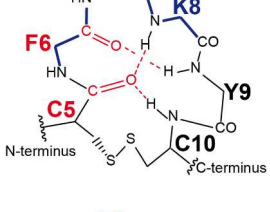
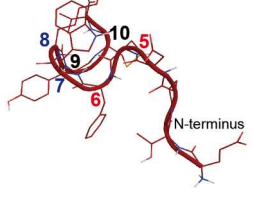
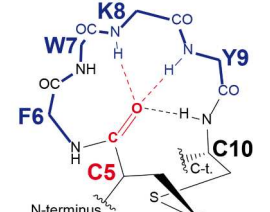
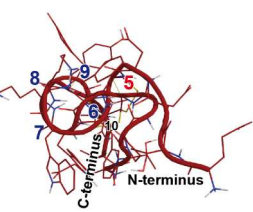
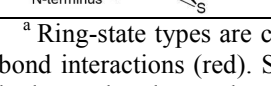
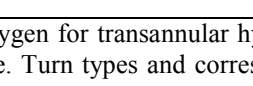
1
2
3 In total 35 μ s of unrestrained MD simulations with the Amber ff99SB force field
4 supplemented with 1.3 μ s CHARMM c36b2 trajectories were used to explore the
5 conformational space of UII (Tables S1 and S2 of the SI). The conformational analysis led to
6 the classification summarized in Table 1. UII exhibits two main types of ring-states, unfolded
7 *open* and saddle-like *folded* ring conformations, which are subdivided into a total of 11
8 subtypes, each defined by its main turn center. Secondary structure propensities and
9 populations of transannular hydrogen bonds are given in Table 2 and 3.

10
11
12
13
14
15
16
17
18 *Open ring-state types.* Turns in this class are centered at residues K⁸Y⁹ or F⁶W⁷ (Table 3)
19 with turns fluctuating around ideal β -turn angles (Table S3 of the SI). The majority of these
20 turns have no or only sparsely populated transannular O_i-H_{i+3} hydrogen bonds (Table 2). Only
21 type *scoop* (6,7 β -I) and *omega-I_{hbond}* (8,9 β -I) exhibit significant transannular hydrogen-bond
22 populations but the latter frequently interconverts with the open *omega-I_{open}* state (8,9 β -VIII)
23 resulting in an average population of 44.3% equivalent to an open turn. Additionally, a ring
24 state was found with no defined β -turns in the ring (*circle*), a loop structure closed by
25 hydrogen bond W⁷O-C⁵H^N. The interpreted structures based on NMR studies of UII in
26 aqueous solution resemble the *open* ring-state types (e.g. turn centers at residues 8,9²² or no
27 transannular hydrogen bonds²⁰). Furthermore, the open *omega* conformations of UII show
28 significant similarities to the *clinched open* states of the related peptide Arg⁸-vasopressin
29 (AVP)⁶² (Table 4). The *clinched open* conformation of AVP, however, is only populated
30 approximately 30% in aqueous solution.⁶¹

31
32
33
34
35
36
37
38
39
40
41
42
43
44
45
46
47 *Folded ring-state types.* The second main cluster comprises *saddle*-like ring conformations
48 with multiple turns, centered either at residues F⁶W⁷K⁸ or W⁷K⁸Y⁹ (Tables 1 and 3). This
49 class shows highly populated transannular hydrogen-bonds that stabilize the *folded*
50 conformations of the ring (Table 2). Subtype *folded-I* (turns centered at W⁷K⁸Y⁹ comprising a
51 7,8 β -I turn) corresponds to the *saddle* state of AVP; subtype *folded-IVb2* (a peptide-bond
52 rotamer of *folded-I* with a 7,8 β -II turn) is equivalent to the *twisted-saddle* state of AVP.
53
54
55
56
57
58
59
60

1
2
3 Interestingly, for AVP, the folded *saddle* conformation is the most highly populated in
4 aqueous solution,^{61, 63} whereas for UII, a folded conformation (β -hairpin centered at W⁷K⁸)
5 has only been identified experimentally in SDS micelles.²⁸ The SDS-conformation resembles
6 the *folded* conformations found in our MD simulations.
7
8
9
10
11
12
13
14
15
16
17
18
19
20
21
22
23
24
25
26
27
28
29
30
31
32
33
34
35
36
37
38
39
40
41
42
43
44
45
46
47
48
49
50
51
52
53
54
55
56
57
58
59
60

Table 1. Classification of Ring Conformations of UII^a

Ring-state type	Turn type	H-bond	Subtype	Cartoon	ID ^b
Open					
Turns centered at KY (8,9)					
	8,9 β-I	⁷ O- ¹⁰ H	<i>omega-I_{hbond}</i>		2
	8,9 β-VIII	open	<i>omega-I_{open}</i>		1
	8,9 β-II	open	<i>omega-II</i>		3
Turns centered at FW (6,7)					
	6,7 β-I	⁵ O- ⁸ H	<i>scoop</i>		5
	6,7 β-I + 4,5 β-I (N-term)	open	<i>lasso</i>		4
Loop without defined turn centers					
	(5-9 loop)	⁹ O- ⁴ H, ⁵ H	<i>circle</i>		10
Folded (saddle-like)					
Multiple turns centered at FWK (6,7,8) or WKY (7,8,9)					
	7,8,9 (7,8 β-I)	⁶ O-(⁹ H, ¹⁰ H)	<i>folded-I</i>		6
	7,8,9 (7,8 β-II)	⁶ O- ⁹ H	<i>folded-IVb2</i>		7
	6,7,8 (5-9 ₃ 10-helix) + 4,5 β-I (N-term)	⁶ O- ⁹ H, ⁵ O-(⁸ H, ¹⁰ H) ³ O- ⁶ H	<i>inv-folded</i>		11
	7,8,9 (6-10 parallel sheet) + 4,5 β-I (N-term)	⁵ O-(⁸ H, ⁹ H, ¹⁰ H) ³ O- ⁶ H	<i>folded-II</i>		8
	6,7,8 (6,7 β-III') + 4,5 β-I (N-term)	⁵ O-(⁸ H, ⁹ H) ³ O- ⁶ H	<i>folded-III</i>		9

^a Ring-state types are characterized by their turn centers (blue) and the donor oxygen for transannular hydrogen-bond interactions (red). Sidechains are indicated by the 1-letter code of the residue. Turn types and corresponding hydrogen bonds populated > 70% are listed.

^b Mean torsion angles (Table S3) and coordinate files of representatives are given in the SI (ID = ID of representative)

1
2
3
4
5
6
7
8
9
10
11
12
13
14
15
16
17
18
19
20
21
22
23
24
25
26
27
28
29
30
31
32
33
34
35
36
37
38
39
40
41
42
43
44
45
46
47
48
49
50
51
52
53
54
55
56
57
58
59
60

Table 2. Hydrogen-Bond Populations^a and Corresponding Turn Centers of UII Ring-State Types

Hydrogen bonds		Conformation (ring-state type)							Turn center
<i>Open</i>									
		Ω - <i>I</i> _{hbond}	Ω - <i>I</i> _{open}	Ω - <i>I</i> _{av} ^b	Ω - <i>II</i>	<i>lasso</i>	<i>scoop</i>	<i>circle</i>	
W ⁷ O	C ¹⁰ H	88.1	18.8	44.3	6.0	0.0	0.0	0.0	8,9
C ⁵ O	K ⁸ H	0.0	0.0	0.0	0.0	12.4	73.8	0.0	6,7
W ⁷ O	Y ⁹ H	9.8	8.5	9.9	0.0	0.7	70.4	0.0	8
Y ⁹ O	C ⁵ H	0.0	0.0	0.0	0.0	0.0	0.0	96.3	(9-5 loop)
Y ⁹ O	D ⁴ H	0.0	0.0	0.0	0.0	0.0	0.0	92.4	(9-4 loop)
<i>Folded</i>									
		<i>folded-I</i>	<i>folded-IVb2</i>	<i>inv-folded</i>	<i>folded-II</i>	<i>folded-III</i>			
F ⁶ O	Y ⁹ H	95.8	73.9	95.8	0.0	0.1			7,8
F ⁶ O	C ¹⁰ H	63.6	10.5	0.0	0.0	0.1			7,8,9
C ⁵ O	K ⁸ H	0.0	2.4	96.1	77.2	83.7			6,7
C ⁵ O	Y ⁹ H	0.0	0.1	0.2	99.4	98.2			6,7,8
C ⁵ O	C ¹⁰ H	0.0	0.0	96.9	89.3	0.3			(5-10)
P ³ O	F ⁶ H	0.9	0.2	68.0	84.3	85.1			4,5
T ² O	W ⁷ H	0.0	0.0	0.0	0.0	61.6			(2-7)

^a Hydrogen-bond populations are relative to the lifetime of the ring state type; only those hydrogen bonds are listed that were found to be populated >50% for at least one ring state subtype; hydrogen bonds > 70% (presumably involved in classical turns) are shown in bold.

^b Average hydrogen-bond population for the frequently interconverting sub-types Ω -*I*_{hbond} and Ω -*I*_{open} (cf. Figure S1 of the SI); Ω = *omega*.

Table 3. Secondary Structure Populations (%) for Ring-State Types of UII

UII										
Ring-state type	Residue ^a									Motif ^b
	T ²	P ³	D ⁴	C ⁵	F ⁶	W ⁷	K ⁸	Y ⁹	C ¹⁰	
<i>Open</i>										
<i>omega-I</i> _{open}	0.00	1.21	1.24	0.66	0.62	0.12	27.12	27.16	1.23	T
<i>omega-I</i> _{hbond}	0.00	24.14	24.15	0.02	0.00	0.00	77.96	78.51	25.05	T
<i>omega-I</i> _{average}	0.10	4.46	4.52	0.17	0.02	0.00	47.41	47.71	15.95	T
<i>omega-II</i>	0.35	2.22	1.88	0.02	0.02	0.00	48.69	48.70	0.52	T
<i>scoop</i>	0.00	3.04	3.04	0.00	86.91	86.94	0.15	7.79	7.79	T
<i>lasso</i>	0.00	0.05	53.99	56.26	21.61	18.36	1.92	1.49	0.00	T
<i>circle</i>	0.00	0.00	0.00	0.00	0.00	0.00	0.00	0.00	0.00	T
<i>Folded</i>										
<i>folded-I</i>	1.02	10.04	11.83	2.50	0.09	75.10	75.22	67.70	3.20	T
<i>folded-IVb2</i>	0.00	4.96	5.22	0.29	0.51	78.78	86.33	68.73	9.36	T
<i>inv-folded</i>	0.00	2.14	59.19	59.19	5.83	6.84	7.84	99.97	89.60	T
	0.00	0.54	20.44	23.31	92.64	93.16	92.15	0.00	0.00	H
<i>folded-II</i>	0.00	0.00	95.07	95.07	42.71	100.00	100.00	98.87	0.00	T
	0.00	0.00	0.00	0.00	57.29	0.00	0.00	0.00	56.47	P
<i>folded-III</i>	24.93	43.33	63.97	64.83	99.90	99.65	99.69	13.04	0.44	T

^a Populations > 75% (classical turns) and > 25% (potentially open turn) are shown in bold and italics, respectively (for notation of secondary structure elements, see SI).

^b T = turn, P = parallel sheet, H = ₃₁₀-helix

Table 4. Similarity of the Ring Torsions of UII₍₅₋₁₀₎, URP₍₂₋₈₎, and AVP₍₁₋₆₎^a

Conformation (ring-state type) ^b			Circular similarity ^c		Turn type		
UII	URP	AVP	UII/URP	UII/AVP	UII	URP	AVP
<i>Open</i>							
1 <i>omega-I_{open}</i>	3r <i>omega-I_{open}</i>	12 <i>cl.open</i>	0.95	0.88	8,9 β-VIII	5,6 β-VIII	4,5 β-VIII _{dist} /I
2 <i>omega-I_{hibond}</i>	1r <i>omega-I_{hibond}</i>	12 <i>cl.open</i>	0.99	0.83	8,9 β-I	5,6 β-I	4,5 β-VIII _{dist} /I
3 <i>omega-II</i>	2r <i>omega-II</i>	-	0.93	-	8,9 β-II	5,6 β-II	4,5 β-II
4 <i>lasso</i>	6r (<i>lasso_{45pbr}</i>)	27 <i>open</i>	0.55 ^d	0.55 ^e	6,7 β-I	3,4 β-VIII _{dist}	2,3
5 <i>scoop</i>	-	-	-	-	6,7 β-I	-	-
10 <i>circle</i>	-	-	-	-	(5-9 loop)	-	-
<i>Folded</i>							
6 <i>folded-I</i>	-	3 <i>saddle</i>	-	0.93	7,8,9 (7,8 β-I)	-	3,4,5 (β-I)
7 <i>folded-IVb2</i>	4r <i>hybrid</i>	19 <i>tw.saddle</i>	0.89	0.95	7,8,9 (7,8 β-II)	4,5,6 γ	3,4,5 (β-II)
	5r <i>sheet</i>	-	0.67	-	-	4,5 (ap.sheet β-II)	-
11 <i>inv-folded</i>	-	-	-	-	6,7,8 (3 ₁₀ -helix)	-	-
8 <i>folded-II</i>	-	-	-	-	7,8,9 (p.sheet)	-	-
9 <i>folded-III</i>	-	-	-	-	6,7,8 (6,7 β-III')	-	-

^a () ring residues.^b coordinate files of UII representative (UII 1 to 11, URP 1r to 6r) are given in the SI; coordinate files of AVP representatives (T16_3,12,19,27) have been published previously⁶².^c circular similarity of corresponding ring torsions (1.00 = identical; for methodological details see SI).^d RMSD_{CA-ring} = 0.714 Å.^e RMSD_{CA-ring} = 0.218 Å (AVP_{open} is a peptide-bond rotamer of UII_{lasso} which has the same backbone shape but a different peptide bond orientation at residues 2,3). Abbreviations: UII human urotensin-II, URP urotensin-related peptide, AVP Arg⁸-vasopressin (representative T16 states⁶²), cl.open = clinched open, ap = antiparallel, p = parallel, dist = distorted, pbr = peptide bond rotamer, inv = inverse.

Are Tail and Ring Conformation of Urotensin-II Mutually Dependent?

As described above, the structure of UII can be characterized by its ring conformation and by treating the N-terminus as an additional residue. A principal-component analysis (PCA) of the overall-torsion space supports this approach. It clusters the overall conformations of UII in accordance to the ring-state types clustered with DASH⁴⁰ (Figure 1). Nevertheless, the tail remains of special interest as it is the only structural difference between UII and URP. DASH clustering (Figures S1 to S6 of the SI) reveals that the basic conformation of the N-terminal tail is *extended* or *folded* with the majority of *folded* tail-conformations caused by a single turn centered at either P³D⁴ or D⁴C⁵ of turn-types β-I/VIII or II, as shown in Figure 2.

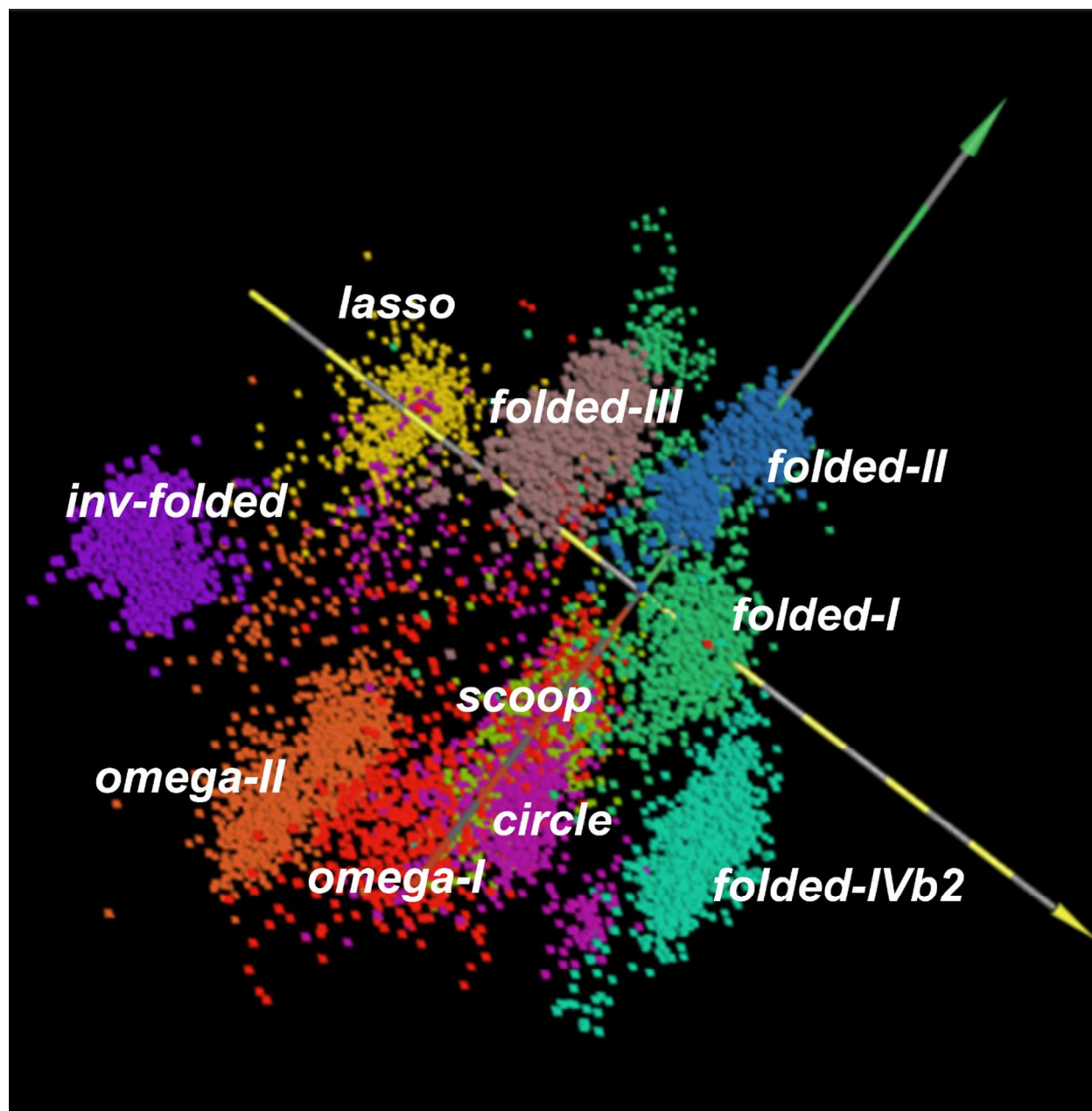


Figure 1. PCA clusters of UII conformations (3D-scatter plot of the three main PCs of the overall backbone torsion space of UII). Each dot represents a conformational snapshot of UII from the MD simulations. Conformations are color-coded by DASH ring-state types. PCA confirms that DASH clustering of ring conformations is suitable for characterizing the overall structure of UII.

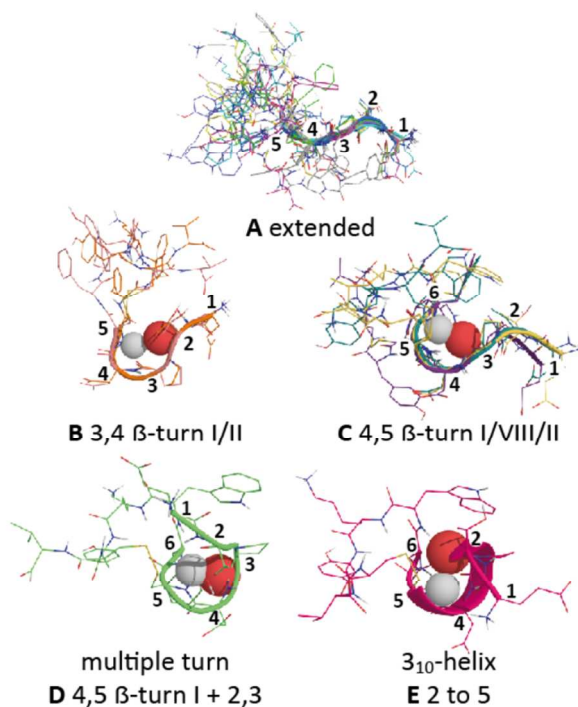


Figure 2. Tail state types of urotensin-II. Hydrogen and oxygen atoms of hydrogen bonds are represented as spheres.

The relative populations of *extended* and *folded* tail-states in the MD simulations vary significantly (cf. Figures S1 to S6 of the SI). Some ring-state types show frequent interconversions of *extended* and *folded* tail states, others none or few; and the *extended:folded* ratio for some types is not consistent between simulations. This raises the question as to whether tail and ring states might be mutually dependent. A qualitative answer is given by analyzing the weights of ring and tail torsions of the main significant PCs for each type of ring conformation (Table S4). If both ring and tail torsions are significantly loaded on one PC, correlation can be assumed. The results are summarized in Table 5. Few ring state types (*folded-I* and *folded-IVb2*) show unambiguously that ring and tail torsions are not correlated, whilst *omega-I* types show uncorrelated ring/tail motions only if the tail is exclusively *extended* (Figure S1). For all other

types, the PCA results suggest interdependence of ring and tail conformations. This contrasts with AVP, where the tail (the three C-terminal residues) moves essentially independently of the ring.⁶² A tentative explanation is the longer tail in UII of four residues facilitates interactions with the ring (e.g. by hydrogen bonding). Mutual dependence of ring and tail conformations is a dynamic property that differentiates UII from URP (no tail) and could modulate different bioactivities.

Table 5. Relative Populations (%),^a Interconversion Frequencies^b and Correlation^c of *Extended* and *Folded* Tail-Conformation for UII Ring-State Types

Ring-state type	Correlation ring/tail	Tail conformation ^d		Interconversion extended/folded	MD ^e
		extended (%)	folded (%)		
<i>omega-I_{hbond/open}</i>	no	100.0 (A)	-	-	I
	yes	38.1 (A)	61.9 (B)	<i>few</i>	III
	yes	37.7 (A)	62.3 (C)	<i>frequent</i>	IV
<i>omega-II</i>	yes	100.0 (A)	-	-	III
	yes	61.9 (A)	38.1 (C)	<i>frequent</i>	XI
<i>scoop</i>	yes	100.0 (A)	-	-	III
<i>lasso</i>	yes	40.8 (A)	59.2 (C)	<i>frequent</i>	IV
<i>circle</i>	yes	100.0 (A)	-	-	IV
<i>folded-I</i>	no	88.6 (A)	11.4 (B)	<i>few</i>	II
<i>folded-IVb2</i>	no	90.2(A)	9.80 (B)	<i>few</i>	III
<i>inv-folded</i>	yes	10.7 (A)	89.3 (C)	<i>few</i>	XI
<i>folded-II</i>	yes	-	100.0 (C)	-	V
<i>folded-III</i>	yes	-	100.0 (D,E,C) ^f	-	V

^a Populations are relative to the length of analyzed sections occupied by single ring-state types in the MD simulations listed. MD = MD simulation (DASH ring and tail-state trajectories are given in Figure S1 to S6 of the SI).

^b cf. DASH tail-state trajectories.

^c Qualitative results from the overall torsion space PCA: If relevant PCs (Eigenvalue > 1.0) correspond to both ring and tail torsions, then correlation was assumed (for details, see SI).

^d Turn types (Figure 2) are in parentheses.

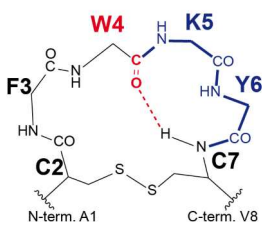
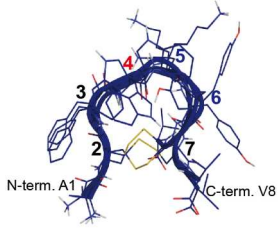
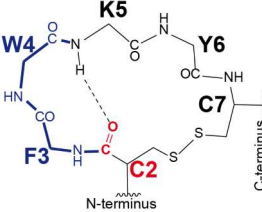
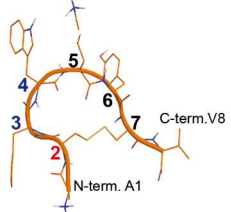
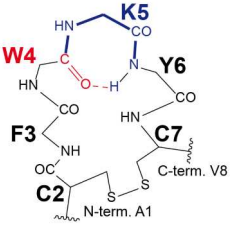
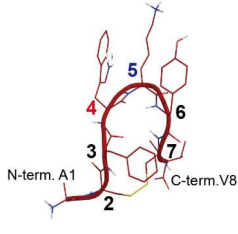
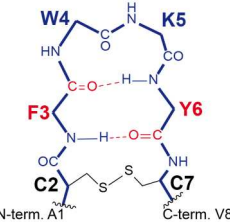
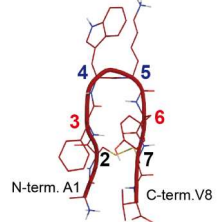
^e MD = MD simulation (DASH ring and tail-state trajectories are given in Figure S1 to S6 of the SI).

^f 40.9%(D) + 32.9%(E) + 26.2%(C).

Conformations of Urotensin Related Peptide.

1
2
3 In total, 22.8 μ s MD were analyzed for URP (Table S1 of the SI). In the MD simulations, the
4 majority of URP conformations (98.4%) belong to the *open* class of *omega* ring-state types
5 (Table 6, Table S3) with the turn centered at residues K⁵ and Y⁶ and a circular similarity of more
6 than 90% to the *omega* states of UII (Table 4). A high similarity of UII and URP ring-
7 conformation was postulated also by Brancaccio et al. based on their NMR studies.³¹ Hydrogen-
8 bond populations at Y⁴O-C⁷H^N and turn propensities at K⁵Y⁶ of URP's *omega type* resemble the
9 data of the corresponding UII conformations (Tables 2 and 3). Conformations with turns
10 different to K⁵Y⁶ are only found as transient states with low absolute populations. There is a
11 variant of the UII *lasso* type with a type VIII β -turn centered at F³W⁴. Two further transient
12 states are comparable with the *folded* conformations of UII. One (denoted as *sheet*) forms an
13 anti-parallel β -sheet with a β -II turn at W⁴K⁵, the other (denoted as *hybrid*) exhibits a γ -turn at
14 W⁴K⁵Y⁶ and shows 89% similarity to the ring torsions of the *folded-IVb2* state of UII. The *sheet*
15 type resembles the postulated single-conformer structure of URP in SDS micelle solution.³¹ The
16 *hybrid* type reminiscent of Chatenet's NMR-based single-conformer description of URP in
17 aqueous solution.¹⁵
18
19
20
21
22
23
24
25
26
27
28
29
30
31
32
33
34
35
36
37
38
39
40
41
42
43
44
45
46
47
48
49
50
51
52
53
54
55
56
57
58
59
60

Table 6. Classification of Ring Conformations of URP^a

<i>Open</i>					
Ring-state type	Turn type	H-bond	Subtype	Cartoon	ID ^b
Turn centered at KY (5,6)					
	5,6 β-I	⁴ O- ⁷ H	<i>omega-I_{hbond}</i>		1r
	5,6 β-VIII	open	<i>omega-I_{open}</i>		3r
	5,6 β-II	open	<i>omega-II</i>		2r
Turns centered at FW (3,4)					
	3,4 β-VIII	open	<i>lasso_{45pbr}</i>		6r
<i>Folded (saddle-like)</i>					
Ring-state type	Turn type	H-bond	Subtype	Cartoon	ID ^b
Turn centered at K (5)					
	4,5,6 γ	⁴ O- ⁶ H	<i>hybrid</i>		4r
turn centered at WK (4,5)					
	2-7 antip. β-sheet (4,5 β-II)	⁶ O- ³ H (³ O- ⁶ H) ^c	<i>sheet</i>		5r

^a Ring-state types are characterized by their turn centers (blue) and the donor oxygen for transannular hydrogen-bond interactions (red). Sidechains are indicated by the single-letter code of the residue. Turn types and corresponding hydrogen bonds populated > 70% are listed.

^b Mean torsion angles (Table S3) and coordinate files of representatives are given in the SI (ID = ID of representative).

^c 48% population.

Determination of UII and URP Equilibrium Populations.

Most of the ring-state types described above exhibit significant lifetimes during MD simulation and, therefore, represent candidates for the main conformations in solution. However, interconversions are too infrequent to derive equilibrium populations directly from the MD simulations. We therefore performed extended REMD simulations of UII and URP to determine the relative population of the states and, hence, to calculate their free energies. NMR experiments were carried out to validate these *in silico* equilibria *via* comparison of calculated and experimental chemical shifts using the statistical metrics reported previously.⁶¹

NMR Experiments.

¹H, ¹³C, and ¹⁵N chemical shifts could be assigned for UII and URP in H₂O at pH 3.0/3.5 and 6.0, with the exception of C and N atoms without directly bonded protons and some rapidly exchangeable H^N atoms at pH 6.0. Our ¹H chemical shifts of UII and URP agree well with those already published^{15, 28, 30, 31} and are complemented by our results for ¹³C and ¹⁵N shifts at the different pH values. The experimental shift lists are given in the SI (Tables S5-S8). The pH was varied to see if changing the protonation state induces significant conformational changes. A change to acidic pH values protonates charged carboxylic acid-containing residues (E¹, D³, and the C-terminal V¹¹ in UII; the C-terminal V⁸ in URP) and this can affect the local electronic structure, as seen by changes in NMR chemical shifts of these residues and their immediate neighbors. The UII peptide is more affected by pH, changing its protonation state from -1 at pH 6.0 to +2 at pH 3.0, whereas URP only changes from +1 at pH 6.0 to +2 at pH 3.0. However, these pH-dependent changes are small compared to those that occur if the solvent is changed

1
2
3 from water to an SDS micelle containing aqueous solution, with no buffer added.^{28, 31} A
4
5 significant conformational change such as that found in SDS micelles^{28,31} can be excluded. Thus,
6
7
8 it can be assumed that the most highly populated conformations of UII and URP at pH 6.0
9
10 resemble the published NMR structures in aqueous solution. We eschewed a further classical
11
12 structure determination using experimental nuclear Overhauser effect (NOE)-distances or
13
14 coupling constants and focused on determining conformational equilibrium concentrations *via* ¹H
15
16 chemical shifts, which proved to be most efficient for vasopressin.⁶¹ In this context, it is
17
18 important to note that, while observed NMR chemical shifts represent the time-average of the
19
20 shifts of all structures in a dynamic equilibrium, this is not true of distances derived from NOE
21
22 peaks. This is because the distance-dependence of the NOE depends on the inverse sixth power
23
24 (r^{-6}),⁶⁴ so that simply averaging the distance (r) will yield incorrect results. Thus, short contacts
25
26 that occur infrequently can give rise to significant NOE peaks, even though the time-averaged
27
28 inter-atom distance may be large. For the same reason, NOE peaks that result from several
29
30 different conformations in equilibrium can masquerade as a single fictitious conformation. A
31
32 second set of resonances representing a minor population (~10% of the total) was also observed
33
34 in the UII NMR spectra. This was identified as the *cis*-Pro³ isomer of UII and fully sequentially
35
36 assigned. As the *cis/trans* conversion in peptides is known to be slow on the NMR timescale^{65, 66}
37
38 it will not contribute to fast equilibria and is not discussed here.
39
40
41
42
43
44
45
46
47
48
49
50

51 **Conformational Equilibrium of Urotensin-II.**

52
53 The relative populations for the representative conformations of UII from three REMD
54
55 simulations (with different initial conformations) are given in Table 7. This table covers
56
57
58
59
60

approximately 80% of the conformational REMD snapshots, the remaining 20% (circular similarity of ring torsions < 65%) are transients that cannot be assigned unambiguously to the representatives. All three REMD simulations predict a similar ratio of *open* to *folded* conformations and, thus, the simulations can be assumed converged for these main conformational types. Unfortunately, the population of the individual sub-types of *open* and *folded* has not converged and differs strongly between the three REMD simulations (Table 7). However, convergence would necessitate significantly longer simulation times which are currently unobtainable.

Table 7. Relative Free Energies ($\Delta\Delta G$, kcal mol⁻¹)^a and Relative Populations (%)^b of Representative Conformations for UII from REMD Simulations

UII representatives		REMD simulations (UII)							
		REMD-I ^c		REMD-II		REMD-III		stddev ^d	
Conformation	ID ^e	$\Delta\Delta G$	pop%	$\Delta\Delta G$	pop%	$\Delta\Delta G$	pop%	$\Delta\Delta G$	pop%
<i>omega-I_{open}</i>	1	0.39	15.19	1.08	8.72	1.09	8.98	±0.33	±2.99
<i>omega-I_{hbond}</i>	2	0.41	14.76	1.45	4.68	1.19	7.69	±0.44	±4.22
<i>omega-II</i>	3	1.04	5.07	2.21	1.29	1.55	4.10	±0.48	±1.61
<i>lasso</i>	4	0.00	29.75	0.00	54.11	0.00	56.73	±0.00	±12.15
<i>scoop</i>	5	1.43	2.67	3.08	0.30	3.37	0.20	±0.85	±1.14
<i>circle</i>	10	1.12	4.53	2.16	1.39	2.08	1.68	±0.47	±1.42
Σ open			72.0		70.5		79.4		
<i>folded-I</i>	6	1.67	1.76	1.71	3.00	2.00	1.82	±0.15	±0.57
<i>folded-IVb2</i>	7	2.28	0.63	3.01	0.34	3.13	0.28	±0.38	±0.15
<i>inv.folded</i>	11	0.35	16.39	1.02	9.67	0.75	15.96	±0.28	±3.07
<i>folded-II</i>	8	1.21	3.89	1.34	5.58	1.84	2.56	±0.27	±1.24
<i>folded-III</i>	9	1.02	5.37	0.95	10.92	-	0.00	±0.04	±4.46
Σ folded			28.0		29.5		20.6		

^a Average standard deviation of all $\Delta\Delta G$ is 0.37 kcal mol⁻¹.

^b Total population of assigned representatives: REMD-I 82%, II 77%, III 87%.

^c The REMD-I equilibrium gives the best agreement with experiment.

^d stddev = standard deviation.

^e Coordinate files are available as SI. ID = ID of representative.

1
2
3 A statistical comparison of the calculated and experimental chemical shifts of UII at pH 6 is
4 given in Table 8. All *open:folded* equilibria of UII correspond better to the experimental values
5 than any single conformation. The best agreement was found for equilibrium REMD-I,
6 predicting a ratio of 72% *open* and 28% *folded* conformations for UII in aqueous solution. A plot
7 of the predicted vs experimental shifts is shown in Figure 3. Correlation of calculated and
8 experimental ^{15}N chemical shifts also confirms the ratio of 72:28 *open* to *folded* as the
9 equilibrium that gives the best agreement, although the number of shifts is very small (Table S14
10 of the SI). The correlation of calculated ^{13}C chemical shifts with experimental shifts is
11 satisfactory for the equilibria but gives the best fit for the *omega-I_{open}* conformations (Table S13
12 of the SI). However, the correlation within the calculated sets of ^{13}C shifts is too high to give
13 unambiguously distinguishable models (Figure S8). This was also found for AVP⁶¹ and is further
14 discussed in the SI.
15
16
17
18
19
20
21
22
23
24
25
26
27
28
29
30

31 Smith and Goodman have proposed the so-called DP4-metric, which they designed specially to
32 discriminate between conformations on the basis of the agreement between calculated and
33 experimental NMR chemical shifts.⁶⁷ The DP4 probability is based on Bayes' theorem and is
34 intended to provide an objective assessment of how likely it is that a given diastereomer (or in
35 our case equilibrium distribution of conformations) is correct based on calculated and
36 experimental chemical shifts. In our case the DP4 probabilities for both ^{13}C and ^1H shifts help
37 confirm that the chemical shift ensemble resulting from equilibrium REMD-I (72:28) has the
38 highest probability of being a correct assignment (Tables S15 of the SI) in comparison to the
39 single conformations or the equilibria REMD-II and -III. Finally, the dependence of DP4 ("best-
40 fit probability") on variations of the *open:folded* ratio also results in a clear maximum for an
41 equilibrium at approximately 70:30 (Figure 4), in accordance with our prediction.
42
43
44
45
46
47
48
49
50
51
52
53
54
55
56
57
58
59
60

Table 8. Statistical Error Values (ppm), Coefficients of Distinctiveness (Δ_{σ}) and Determination (R^2) for the Linear Regression of Calculated and Experimental ^1H Chemical Shifts of UII in Aqueous Solution at pH 6.0

UII representatives and equilibria (<i>open:folded</i>)	MSE	MUE	RMSD	WRMSE	Δ_{σ}	R^2
<i>omega-I_{open}</i>	-0.09	0.38	0.51	0.56	1.11	0.934
<i>omega-I_{hbond}</i>	-0.02	0.31	0.42	0.46	0.99	0.956
<i>omega-II</i>	0.03	0.33	0.43	0.46	1.02	0.953
<i>lasso</i>	0.03	0.29	0.35	0.38	0.96	0.968
<i>scoop</i>	0.03	0.41	0.50	0.54	1.26	0.938
<i>circle</i>	0.00	0.30	0.40	0.42	0.95	0.962
<i>folded-I</i>	0.04	0.32	0.39	0.43	1.06	0.963
<i>folded-IVb2</i>	0.11	0.32	0.39	0.40	1.01	0.966
<i>inv-folded</i>	0.06	0.34	0.42	0.44	1.14	0.955
<i>folded-II</i>	0.05	0.40	0.49	0.55	1.15	0.936
<i>folded-III</i>	-0.04	0.37	0.45	0.50	1.19	0.946
Equilibrium REMD-I (72:28)	0.01	0.21	0.26	0.27	0.75	0.982
Equilibrium REMD-II (70:30)	0.01	0.22	0.28	0.29	0.78	0.980
Equilibrium REMD-III (79:21)	0.02	0.23	0.29	0.30	0.81	0.979

The best results are shown in bold. MSE = Mean Square Error; MUE = Mean Unsigned Error; RMSD = Root Mean Square Deviation; WRMSE = Weighted Root MSE; Δ_{σ} = coefficient of distinctiveness;⁶¹ R^2 = coefficient of determination

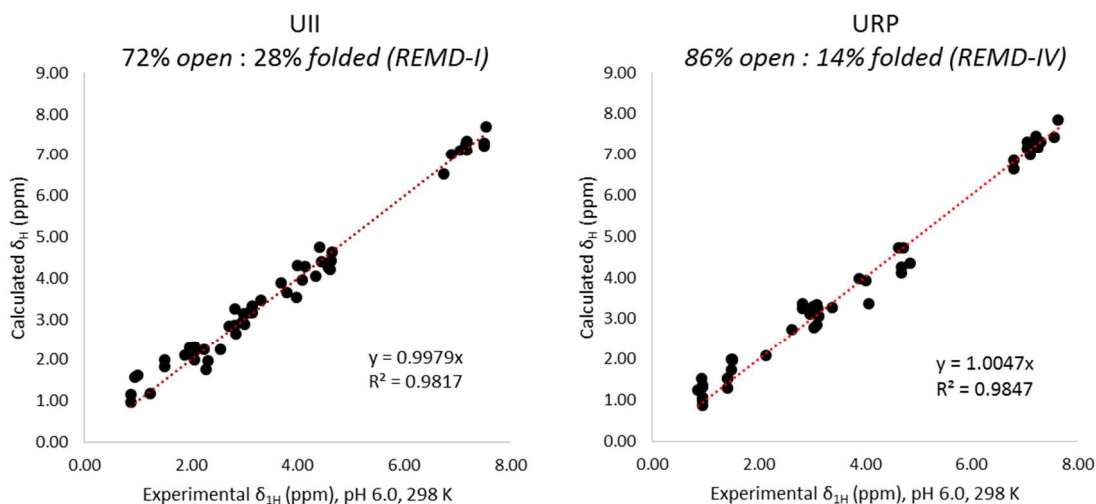


Figure 3. Linear regression of calculated ^1H chemical shifts for the best predicted equilibria of *open* and *folded* conformations of UII and URP against experimental chemical shifts of non-exchangeable ^1H of UII and URP in aqueous solution at pH 6.0, 298K.

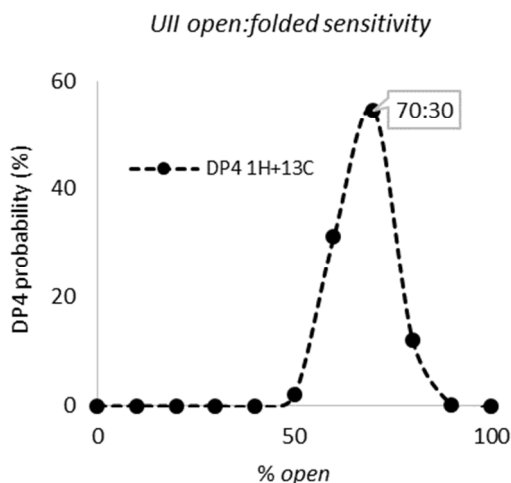


Figure 4. Dependence of DP4 probabilities on the *open:folded* ratio of UII. *Open* and *folded* subtype mixtures correspond to the relative concentrations of the 11-component equilibrium REMD-I. The maximum probability (most likely ratio) is approximately 70:30 *open:folded*.

Besides the experimental shifts of UII at pH 6, a second set of experimental shifts at pH 3 was measured and compared with the calculated shifts. The statistical metrics (data not shown) are extremely close to those at pH 6 which suggests conformational independence of UII for different protonation states (+2 at pH 3, -1 at pH 6).

The seemingly contradictory experimental single-conformer interpretations of UII's structure in H₂O (no classical turns²⁸ vs widened 7,8,9+8,9,10 γ -turns³⁰) are more precisely a fast (on the NMR timescale) equilibrium of major *open* and minor *folded* ring-conformations, rather than any single conformation. A *folded* conformation has so far only been proposed from NMR

1
2
3 experiments in SDS micelles, and was suggested to be the bioactive conformation in the UII
4 receptor (UTR).²⁸ Our results indicate that the proposed bioactive *folded*-type conformations
5
6 already exist in aqueous solution to a significant extent, hidden in the fast equilibrium and that, if
7
8 it is the bioactive conformation, it is selected by preferential binding to the receptor from the
9
10 conformational ensemble.
11
12
13
14
15
16
17
18
19

20 **Conformational Equilibrium of Urotensin Related Peptide.**

21
22 Three REMD simulations of URP starting from different initial conformations gave the
23 relative free energies and populations listed in Table 9. The representatives cover approximately
24 70% of all REMD conformations. The remaining 30% (circular similarity of ring torsions <
25 65%) are transient conformations that could not be assigned unambiguously. The overall ratio of
26
27 *open:folded* conformations from different REMD simulations are again similar and can be
28
29 regarded as converged.
30
31
32
33
34
35
36
37
38
39
40
41
42
43
44
45
46
47
48
49
50
51
52
53
54
55
56
57
58
59
60

Table 9. Relative Free Energies ($\Delta\Delta G$, kcal mol⁻¹)^a and Relative Populations (%)^b of Representative Conformations for URP from three different REMD Simulations^{a,b,c}

URP representatives		REMD simulations (URP)							
Conformation	ID ^c	REMD-IV ^c		REMD-V		REMD-VI		stddev ^d	
		$\Delta\Delta G$	%	$\Delta\Delta G$	%	$\Delta\Delta G$	%	$\Delta\Delta G$	%
<i>omega-I_{open}</i>	3r	0.34	18.92	1.38	5.80	0.45	19.70	±0.47	±6.38
<i>omega-I_{hbond}</i>	1r	0.08	29.73	0.49	26.09	0.33	24.24	±0.17	±2.28
<i>omega-II</i>	2r	0.00	33.78	0.00	59.42	0.00	42.42	±0.00	±10.65
<i>lasso</i>	6r	1.26	4.05	1.79	2.90	1.32	4.55	±0.24	±0.69
Σ open		86.5		94.2		90.9			
<i>sheet</i>	5r	0.71	10.14	1.38	5.80	1.73	2.27	±0.42	±3.22
<i>hybrid</i>	4r	1.36	3.38	-	0.00	1.08	6.82	±0.14	±2.78
Σ folded		13.5		5.8		9.1			

^a Average standard deviation 0.29 kcal mol⁻¹.

^b Total population of assigned representatives: REMD-IV 74%, V 69%, VI 66%.

^c The REMD-IV equilibrium gives the best agreement with experiment.

^d stddev = standard deviation.

^e Coordinate files are available as SI. ID = ID of representative.

Table 10. Statistical Error Values (ppm), Coefficients of Distinctiveness (Δ_{σ}) and Determination (R^2) for the Linear Regression of Calculated and Experimental ¹H Chemical Shifts of URP in Aqueous Solution at pH 6.0

URP representatives and equilibria (<i>open:folded</i>)	MSE	MUE	RMSD	WRMSE	Δ_{σ}	R^2
<i>omega-I_{open}</i>	-0.02	0.27	0.37	0.43	1.02	0.9774
<i>omega-I_{hbond}</i>	-0.09	0.32	0.44	0.55	0.99	0.9624
<i>omega-II</i>	-0.11	0.40	0.53	0.64	1.20	0.9456
<i>lasso</i>	-0.08	0.41	0.52	0.64	1.26	0.9489
<i>sheet</i>	-0.05	0.28	0.38	0.43	1.01	0.9755
<i>hybrid</i>	-0.01	0.33	0.44	0.53	1.12	0.9666
Equilibrium REMD-IV (86:14)	-0.08	0.22	0.29	0.31	0.78	0.9847
Equilibrium REMD-V (94:6)	-0.10	0.29	0.38	0.44	0.91	0.9723
Equilibrium REMD-VI (91:9)	-0.08	0.25	0.31	0.35	0.84	0.9815

The best results are shown in bold. MSE = Mean Square Error; MUE = Mean Unsigned Error; RMSD = Root Mean Square Deviation; WRMSE = Weighted Root MSE; Δ_{σ} = coefficient of distinctiveness; R^2 = coefficient of determination

The model that agrees best with experiment is the equilibrium from REMD-IV (calculated ¹H chemical shifts for URP are given in Table S12 of the SI) predicting a ratio of 86% *open* and

1
2
3 14% *folded* conformations for URP with a predominance of *omega* conformations (Table 10,
4 Figure 3). This result is further supported by the DP4 assignment probabilities (Tables S15).
5
6

7
8 Equilibrium REMD-VI also performs better than any single conformation. Only equilibrium
9
10 REMD-V fits worse than the *omega-I_{open}* conformation. It is noteworthy that the average ratio of
11
12 the frequently interconverting conformations *omega-I_{open}* and *omega-I_{hbond}* in the long-scale MD
13
14 simulations is 42:58. This resembles the relative populations of REMD-IV (39:61) and VI
15
16 (45:55), but not REMD-V (18:82). Insufficient convergence of the *omega-I_{open}:omega-I_{hbond}* ratio
17
18 may explain the poor performance of equilibrium REMD-V.
19
20
21
22
23

24
25 How do the conformational equilibria of URP and UII differ? Both exhibit predominantly *open*
26
27 conformations in aqueous solution but UII shows a higher population of *folded* conformations
28
29 (UII: 28%, URP: 14%). This result is consistent with the possible interdependence of ring and
30
31 tail conformation in UII but not URP, and supports the hypothesis that the N-terminal tail
32
33 facilitates the formation of *folded* ring conformations.
34
35
36
37
38

39 CONCLUSIONS

40
41 Conformation and dynamics of UII and URP in aqueous solution were explored and classified
42
43 by combining computational and experimental methods. The two peptides exhibit similar ring
44
45 conformations. The structures of both UII and URP in aqueous solution cannot be described by
46
47 single conformations. As found previously for Arg⁸-vasopressin,⁶¹ UII and URP exist in solution
48
49 in a conformational equilibrium between *open* and *folded* (saddle-like) ring conformations and in
50
51 combination with *extended* and *folded* tail conformations. In contrast to vasopressin, however,
52
53 the ring and tail conformations of UII are not independent of each other, so that UII behaves
54
55 differently to URP, as URP lacks the tail region. *Folded* (saddle-like) conformations of URP
56
57
58
59
60

1
2
3 appear only transiently in unrestricted MD simulations and the equilibrium distribution of
4 conformations that results from REMD simulations and agrees best with experimental ¹H
5 chemical shifts is 86% *open* : 14% *folded*. The corresponding equilibrium for UII is
6 72% *open* : 28% *folded*. These data suggest that the free-energy penalty for a possible *folded*
7 biologically active conformation is approximately 1.1 kcal mol⁻¹ for URP but considerably
8 smaller (approximately 0.6 kcal mol⁻¹) for UII, probably because of ring-tail interactions in UII.
9 This difference may be significant in determining different effects of the two peptides on binding
10 to the UII-receptor (UT2SR, UTR). The high similarity of ring-conformations of UII and URP
11 support Brancaccio's finding³¹ that differences in the biological function are not related to
12 differences in ring-conformations. UII and URP show the same conformational main-types as the
13 structurally related GPCR-ligand Arg⁸-vasopressin. However, both prefer *open*-type
14 conformations in solution, in strong contrast to AVP (70% *folded* conformations).
15
16
17
18
19
20
21
22
23
24
25
26
27
28
29
30

31 All thermodynamically accessible representative conformations of UII and URP can serve as
32 templates for 3D ligand-based drug design or docking, the structural data are given in the SI.
33
34

35 The NMR data reported here supplement and complete published data. They include an almost
36 complete assignment of the spectra of the *cis*-Pro³ isomers of UII. We have developed a novel
37 and robust procedure to extract conformational equilibria from NMR data by combining
38 experiment with enhanced sampling simulations. The protocol was developed on AVP⁶¹ and
39 tested here on UII and URP. It seems a powerful tool for exploring the conformational equilibria
40 of intrinsically flexible peptides. In the case of UII and URP, we have used REMD to determine
41 the calculated equilibrium concentrations, rather than the metadynamics procedure used for
42 AVP. Future work will evaluate a variety of enhanced-sampling protocols in order to determine
43 the most suitable for peptide conformational equilibria.
44
45
46
47
48
49
50
51
52
53
54
55
56
57
58
59
60

1
2
3 The protocol tested and published⁶¹ for Arg⁸-vasopressin and based on proton chemical shifts
4 also yields well-defined predictions for UII and URP, here using REMD to determine the
5
6 calculated equilibrium concentrations.
7
8

9
10 Unfortunately, we have little information about the lifetimes of the individual conformations.
11
12 The conformational equilibria are fast on the NMR time scale but too slow for us to be able to
13
14 sample them adequately in unbiased simulations.
15
16
17
18
19

20 ASSOCIATED CONTENT

21 Supporting Information

22
23 Details of MD simulations, conformational analysis, principal component analysis, NMR
24
25 experiments, DFT calculations, REMD equilibrium models, ¹³C linear regression, sensitivity
26
27 analysis of metrics, ¹⁵N linear regression, tables of experimental and calculated ¹H, ¹³C, ¹⁵N
28
29 chemical shifts, coordinate files of representatives. This material is available free of charge via
30
31 the Internet at <http://pubs.acs.org>.
32
33
34
35
36

37 AUTHOR INFORMATION

38 Corresponding Author

39
40
41 *E-mail: tim.clark@fau.de
42
43

44 Notes

45
46 The authors declare no competing financial interest.
47
48
49
50
51
52

53 ACKNOWLEDGMENTS

54
55 This work was supported by the European project “Peptide Research Network of Excellence”
56
57 PeReNE as part of the Interreg IVA France (Channel) – England 2007 2014 program (Interreg
58
59
60

1
2
3 EU). NM, MM, and JWE are grateful to AstraZeneca for their support. We thank Helene Castel
4
5 and Jérôme Leprince (University of Rouen, France) for helpful discussions. Isabelle Milazzo
6
7 (University of Rouen, France) is acknowledged for providing NMR-structures of hUII and URP
8
9 for the CHARMM simulations.
10
11
12
13
14
15
16
17
18
19
20
21
22
23
24
25
26
27
28
29
30
31
32
33
34
35
36
37
38
39
40
41
42
43
44
45
46
47
48
49
50
51
52
53
54
55
56
57
58
59
60

REFERENCES

1. Bern, H. A.; Lederis, K., A Reference Preparation for the Study of Active Substances in the Caudal Neurosecretory System of Teleosts. *J. Endocrin.* **1969**, 45, Suppl:xi-xii.
2. Ames, R. S.; Sarau, H. M.; Chambers, J. K.; Willette, R. N.; Aiyar, N. V.; Romanic, A. M.; Loudon, C. S.; Foley, J. J.; Sauermelch, C. F.; Coatney, R. W.; Ao, Z.; Disa, J.; Holmes, S. D.; Stadel, J. M.; Martin, J. D.; Liu, W. S.; Glover, G. I.; Wilson, S.; McNulty, D. E.; Ellis, C. E.; Elshourbagy, N. A.; Shabon, U.; Trill, J. J.; Hay, D. W.; Ohlstein, E. H.; Bergsma, D. J.; Douglas, S. A., Human Urotensin-II is a Potent Vasoconstrictor and Agonist for the Orphan Receptor GPR14. *Nature* **1999**, 401, 282-286.
3. Marchese, A.; Heiber, M.; Nguyen, T.; Heng, H. H.; Saldivia, V. R.; Cheng, R.; Murphy, P. M.; Tsui, L. C.; Shi, X.; Gregor, P.; et al., Cloning and Chromosomal Mapping of Three Novel Genes, GPR9, GPR10, and GPR14, Encoding Receptors Related to Interleukin 8, Neuropeptide Y, and Somatostatin Receptors. *Genomics* **1995**, 29, 335-344.
4. Mori, M.; Sugo, T.; Abe, M.; Shimomura, Y.; Kurihara, M.; Kitada, C.; Kikuchi, K.; Shintani, Y.; Kurokawa, T.; Onda, H.; Nishimura, O.; Fujino, M., Urotensin II is the endogenous ligand of a G-protein-coupled orphan receptor, SENR (GPR14). *Biochem. Biophys. Res. Communications* **1999**, 265, 123-129.
5. Nothacker, H. P.; Wang, Z.; McNeill, A. M.; Saito, Y.; Merten, S.; O'Dowd, B.; Duckles, S. P.; Civelli, O., Identification of the Natural Ligand of an Orphan G-Protein-Coupled Receptor Involved in the Regulation of Vasoconstriction. *Nat. Cell Biol.* **1999**, 1, 383-385.
6. Liu, Q.; Pong, S. S.; Zeng, Z.; Zhang, Q.; Howard, A. D.; Williams, D. L., Jr.; Davidoff, M.; Wang, R.; Austin, C. P.; McDonald, T. P.; Bai, C.; George, S. R.; Evans, J. F.; Caskey, C. T., Identification of Urotensin II as the Endogenous Ligand for the Orphan G-Protein-Coupled Receptor GPR14. *Biochem. Biophys. Res. Commun.* **1999**, 266, 174-178.
7. Vaudry, H.; Do Rego, J. C.; Le Mevel, J. C.; Chatenet, D.; Tostivint, H.; Fournier, A.; Tonon, M. C.; Pelletier, G.; Conlon, J. M.; Leprince, J., Urotensin II, From Fish to Human. *Phylogenetic Aspects of Neuropeptides: From Invertebrates to Humans* **2010**, 1200, 53-66.
8. Vaudry, H.; Leprince, J.; Chatenet, D.; Fournier, A.; Lambert, D. G.; Le Mevel, J. C.; Ohlstein, E. H.; Schwertani, A.; Tostivint, H.; Vaudry, D., International Union of Basic and Clinical Pharmacology. XCII. Urotensin II, Urotensin II-Related Peptide, and their Receptor: From Structure to Function. *Pharmacol. Rev.* **2015**, 67, 214-258.
9. Tostivint, H.; Quan, F. B.; Bougerol, M.; Kenigfest, N. B.; Lihmann, I., Impact of Gene/Genome Duplications on the Evolution of the Urotensin II and Somatostatin Families. *Gen Comp. Endocrinol.* **2013**, 188, 110-117.
10. Merlino, F.; Di Maro, S.; Munaim Yousif, A.; Caraglia, M.; Grieco, P., Urotensin-II Ligands: An Overview from Peptide to Nonpeptide Structures. *J Amino Acids* **2013**, 2013, 979016.
11. Tostivint, H.; Ocampo Daza, D.; Bergqvist, C. A.; Quan, F. B.; Bougerol, M.; Lihmann, I.; Larhammar, D., Molecular Evolution of GPCRs: Somatostatin/Urotensin II Receptors. *J. Mol. Endocrinol.* **2014**, 52, T61-86.
12. Sugo, T.; Murakami, Y.; Shimomura, Y.; Harada, M.; Abe, M.; Ishibashi, Y.; Kitada, C.; Miyajima, N.; Suzuki, N.; Mori, M.; Fujino, M., Identification of Urotensin II-Related Peptide as the Urotensin II-Immunoreactive Molecule in the Rat Brain. *Biochem. Biophys. Res. Commun.* **2003**, 310, 860-868.

- 1
2
3
4
5
6
7
8
9
10
11
12
13
14
15
16
17
18
19
20
21
22
23
24
25
26
27
28
29
30
31
32
33
34
35
36
37
38
39
40
41
42
43
44
45
46
47
48
49
50
51
52
53
54
55
56
57
58
59
60
13. Chatenet, D.; Nguyen, T. T.; Letourneau, M.; Fournier, A., Update on the Urotensinergic System: New Trends in Receptor Localization, Activation, and Drug Design. *Front. Endocrinol.* **2012**, 3-3.
 14. Zhu, Y. C.; Zhu, Y. Z.; Moore, P. K., The Role of Urotensin II in Cardiovascular and Renal Physiology and Diseases. *Br. J. Pharmacol.* **2006**, 148, 884-901.
 15. Chatenet, D.; Dubessy, C.; Leprince, J.; Boularan, C.; Carlier, L.; Ségalas-Milazzo, I.; Guilhaudis, L.; Oulyadi, H.; Davoust, D.; Scalbert, E.; Pfeiffer, B.; Renard, P.; Tonon, M.-C.; Lihrmann, I.; Pacaud, P.; Vaudry, H., Structure–Activity Relationships and Structural Conformation of a Novel Urotensin II-Related Peptide. *Peptides* **2004**, 25, 1819-1830.
 16. Labarrere, P.; Chatenet, D.; Leprince, J.; Marionneau, C.; Loirand, G.; Tonon, M. C.; Dubessy, C.; Scalbert, E.; Pfeiffer, B.; Renard, P.; Calas, B.; Pacaud, P.; Vaudry, H., Structure-Activity Relationships of Human Urotensin II and Related Analogues on Rat Aortic Ring Contraction. *J. Enz. Inhibit. Med. Chem.* **2003**, 18, 77-88.
 17. Bucharles, C.; Bizet, P.; Arthaud, S.; Arabo, A.; Leprince, J.; Lefranc, B.; Cartier, D.; Anouar, Y.; Lihrmann, I., Concordant Localization of Functional Urotensin II and Urotensin II-Related Peptide Binding Sites in the Rat Brain: Atypical Occurrence Close to the Fourth Ventricle. *J. Comp. Neurol.* **2014**, 522, 2634-2649.
 18. Douglas, S. A.; Naselsky, D.; Ao, Z.; Disa, J.; Herold, C. L.; Lynch, F.; Aiyar, N. V., Identification and Pharmacological Characterization of Native, Functional Human Urotensin-II Receptors in Rhabdomyosarcoma Cell Lines. *Br. J. Pharmacol.* **2004**, 142, 921-932.
 19. Jarry, M.; Diallo, M.; Lecointre, C.; Desrues, L.; Tokay, T.; Chatenet, D.; Leprince, J.; Rossi, O.; Vaudry, H.; Tonon, M. C.; Prezeau, L.; Castel, H.; Gandolfo, P., The Vasoactive Peptides Urotensin II and Urotensin II-Related Peptide Regulate Astrocyte Activity Through Common and Distinct Mechanisms: Involvement in Cell Proliferation. *Biochem. J.* **2010**, 428, 113-124.
 20. Ashton, N., Renal and Vascular Actions of Urotensin II. *Kidney Int.* **2006**, 70, 624-629.
 21. Stirrat, A.; Gallagher, M.; Douglas, S. A.; Ohlstein, E. H.; Berry, C.; Kirk, A.; Richardson, M.; MacLean, M. R., Potent Vasodilator Responses to Human Urotensin-II in Human Pulmonary and Abdominal Resistance Arteries. *Am. J. Physiol. Heart Circ. Physiol.* **2001**, 280, H925-928.
 22. Chatenet, D.; Letourneau, M.; Nguyen, Q.; Doan, N.; Dupuis, J.; Fournier, A., Discovery of New Antagonists Aimed at Discriminating UII and URP-mediated Biological Activities: Insight into UII and URP Receptor Activation. *Br. J. Pharmacol.* **2013**, 168, 807-821.
 23. Kinney, W. A.; Almond Jr, H. R.; Qi, J.; Smith, C. E.; Santulli, R. J.; de Garavilla, L.; Andrade-Gordon, P.; Cho, D. S.; Everson, A. M.; Feinstein, M. A.; Leung, P. A.; Maryanoff, B. E., Structure-Function Analysis of Urotensin II and its Use in the Construction of a Ligand-Receptor Working Model. *Angew. Chem. Int. Ed. Engl.* **2002**, 41, 2940-2940.
 24. Flohr, S.; Kurz, M.; Kostenis, E.; Brkovich, A.; Fournier, A.; Klabunde, T., Identification of Nonpeptidic Urotensin II Receptor Antagonists by Virtual Screening Based on a Pharmacophore Model Derived from Structure–Activity Relationships and Nuclear Magnetic Resonance Studies on Urotensin II. *J. Med. Chem.* **2002**, 45, 1799-1805.
 25. Foister, S.; Taylor, L. L.; Feng, J. J.; Chen, W. L.; Lin, A.; Cheng, F. C.; Smith, A. B., 3rd; Hirschmann, R., Design and Synthesis of Potent Cystine-Free Cyclic Hexapeptide Agonists at the Human Urotensin Receptor. *Org. Lett.* **2006**, 8, 1799-1802.

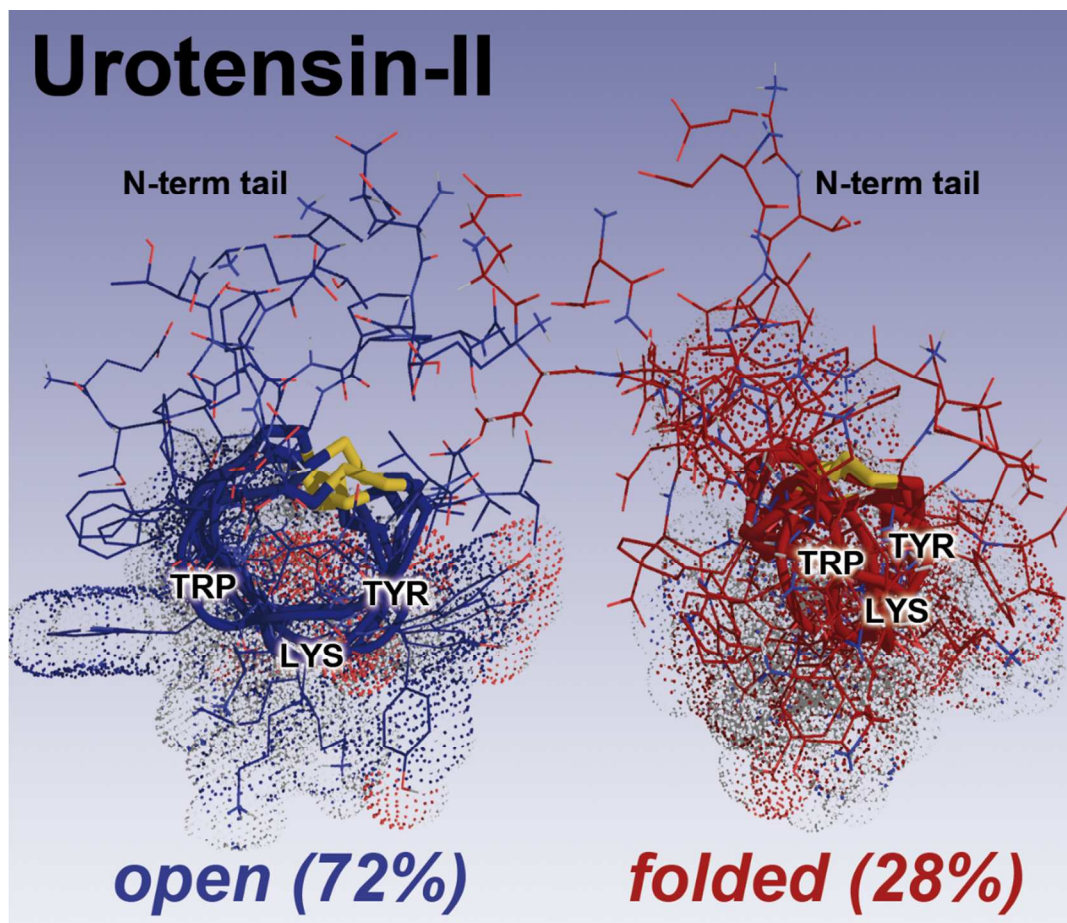
- 1
2
3 26. McMaster, D.; Kobayashi, Y.; Rivier, J.; Lederis, K., Characterization of the Biologically
4 and Antigenically Important Regions of Urotensin II. *Proc. West. Pharmacol. Soc.* **1986**, *29*,
5 205-208.
- 6
7 27. Bandholtz, S.; Erdmann, S.; von Hacht, J. L.; Exner, S.; Krause, G.; Kleinau, G.;
8 Gröttinger, C., Urolinin: The First Linear Peptidic Urotensin-II Receptor Agonist. *J. Med. Chem.*
9 **2016**, *59*, 10100-10112.
- 10 28. Carotenuto, A.; Grieco, P.; Campiglia, P.; Novellino, E.; Rovero, P., Unraveling the
11 Active Conformation of Urotensin II. *J. Med. Chem.* **2004**, *47*, 1652-1661.
- 12 29. Grieco, P.; Carotenuto, A.; Patacchini, R.; Maggi, C. A.; Novellino, E.; Rovero, P.,
13 Design, Synthesis, Conformational Analysis, and Biological Studies of Urotensin-II Lactam
14 Analogues. *Bioorg. Med. Chem.* **2002**, *10*, 3731-3739.
- 15 30. Lescot, E.; Sopkova-de Oliveira Santos, J.; Dubessy, C.; Oulyadi, H.; Lesnard, A.;
16 Vaudry, H.; Bureau, R.; Rault, S., Definition of New Pharmacophores for Nonpeptide
17 Antagonists of Human Urotensin-II. Comparison with the 3D-Structure of Human Urotensin-II
18 and URP. *J. Chem. Inf. Model.* **2007**, *47*, 602-612.
- 19 31. Brancaccio, D.; Merlino, F.; Limatola, A.; Yousif, A. M.; Gomez-Monterrey, I.;
20 Campiglia, P.; Novellino, E.; Grieco, P.; Carotenuto, A., An Investigation into the Origin of the
21 Biased Agonism Associated with the Urotensin II Receptor Activation. *J. Pept. Sci.* **2015**, *21*,
22 392-399.
- 23 32. Case, D. A.; Cheatham, T. E.; Darden, T.; Gohlke, H.; Luo, R.; Merz, K. M.; Onufriev,
24 A.; Simmerling, C.; Wang, B.; Woods, R. J., The Amber Biomolecular Simulation Programs. *J.*
25 *Comput. Chem.* **2005**, *26*, 1668-1688.
- 26 33. Case, D. A.; Darden, T. A.; Cheatham II, T. E.; Simmerling, C. L.; Wang, J.; Duke, R. E.;
27 R. Luo; Crowley, M.; C. Walker, R.; Zhang, W.; Merz, K. M.; B. Wang; S. Hayik; Roitberg, A.;
28 G. Seabra; Kolossváry, I.; F. Wong, K.; Paesani, F.; Vanicek, J.; Wu, X.; Brozell, S. R.;
29 Steinbrecher, T.; Gohlke, H.; Yang, L.; Tan, C.; Mongan, J.; Hornak, V.; Cui, G.; Mathews, D.
30 H.; Seetin, M. G.; Sagui, C.; V. Babin; Kollman, P. A. *AMBER 10*, 2008.
- 31 34. Case, D. A.; Babin, V.; Berryman, J. T.; Betz, R. M.; Cai, Q.; Cerutti, D. S.; Cheatham,
32 T. E. I.; Darden, T. A.; Duke, R. E.; Gohlke, H.; Goetz, A. W.; Gusarov, S.; Homeyer, N.;
33 Janowski, P.; Kaus, J.; Kolossváry, I.; Kovalenko, A.; Lee, T. S.; LeGrand, S.; Luchko, T.; Luo,
34 R.; Madej, B. D.; Merz, K. M.; Paesani, F.; Roe, D. R.; Roitberg, A.; Sagui, C.; Salomon-Ferrer,
35 R.; Seabra, G. M.; Simmerling, C. L.; Smith, W. S.; Swails, J.; Walker, R. C.; Wang, J.; Wolf, R.
36 M.; Wu, X.; Kollman, P. A. *AMBER 14*, 2014.
- 37 35. Salomon-Ferrer, R.; Götz, A. W.; Poole, D.; Le Grand, S.; Walker, R. C., Routine
38 Microsecond Molecular Dynamics Simulations with AMBER on GPUs. 2. Explicit Solvent
39 Particle Mesh Ewald. *J. Chem. Theor. Comput.* **2013**, *9*, 3878-3888.
- 40 36. Goetz, A. W.; Williamson, M. J.; Xu, D.; Poole, D.; Le Grand, S.; Walker, R. C., Routine
41 Microsecond Molecular Dynamics Simulations with AMBER on GPUs. 1. Generalized Born. *J.*
42 *Chem. Theor. Comput.* **2012**, *8*, 1542-1555.
- 43 37. Le Grand, S.; Goetz, A. W.; Walker, C. R., SPFP: Speed without Compromise - A Mixed
44 Precision Model for GPU Accelerated Molecular Dynamics Simulations. *Comp. Phys. Comm.*
45 **2013**, *184*, 374-380.
- 46 38. Brooks, B. R.; Brooks, C. L., 3rd; Mackerell, A. D., Jr.; Nilsson, L.; Petrella, R. J.; Roux,
47 B.; Won, Y.; Archontis, G.; Bartels, C.; Boresch, S.; Caflisch, A.; Caves, L.; Cui, Q.; Dinner, A.
48 R.; Feig, M.; Fischer, S.; Gao, J.; Hodoscek, M.; Im, W.; Kuczera, K.; Lazaridis, T.; Ma, J.;
49 Ovchinnikov, V.; Paci, E.; Pastor, R. W.; Post, C. B.; Pu, J. Z.; Schaefer, M.; Tidor, B.; Venable,
50
51
52
53
54
55
56
57
58
59
60

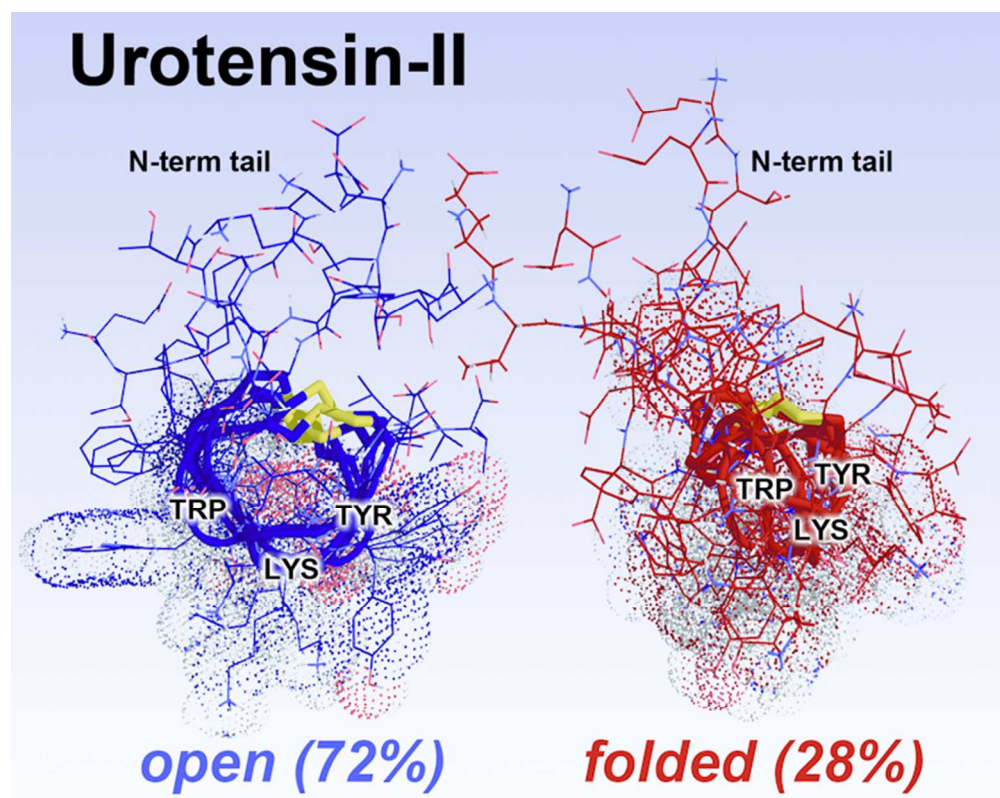
- 1
2
3 R. M.; Woodcock, H. L.; Wu, X.; Yang, W.; York, D. M.; Karplus, M., CHARMM: The
4 Biomolecular Simulation Program. *J. Comput. Chem.* **2009**, 30, 1545-614.
- 5
6 39. Hornak, V.; Abel, R.; Okur, A.; Strockbine, B.; Roitberg, A.; Simmerling, C.,
7 Comparison of Multiple Amber Force Fields and Development of Improved Protein Backbone
8 Parameters. *Proteins: Struct. Funct. Bioinf.* **2006**, 65, 712-725.
- 9
10 40. Salt, D. W.; Hudson, B. D.; Banting, L.; Ellis, M. J.; Ford, M. G., DASH: A Novel
11 Analysis Method for Molecular Dynamics Simulation Data. Analysis of Ligands of PPAR-
12 Gamma. *J. Med. Chem.* **2005**, 48, 3214-3220.
- 13
14 41. DASH 1.0.-2.11. www.port.ac.uk/research/cmd/software (accessed Sep, 2014 - March,
15 **2016**)
- 16
17 42. Case, D. A.; Darden, T. A.; Cheatham II, T. E.; Simmerling, C. L.; Wang, J.; Duke, R. E.;
18 R. Luo; Crowley, M.; C.Walker, R.; Zhang, W.; Merz, K. M.; B.Wang; S. Hayik; Roitberg, A.;
19 G. Seabra; Kolossváry, I.; F.Wong, K.; Paesani, F.; Vanicek, J.; Wu, X.; Brozell, S. R.;
20 Steinbrecher, T.; Gohlke, H.; Yang, L.; Tan, C.; Mongan, J.; Hornak, V.; Cui, G.; Mathews, D.
21 H.; Seetin, M. G.; Sagui, C.; V. Babin; Kollman, P. A. *AmberTools 1.0*, AmberTools 1.0; **2008**.
- 22
23 43. Kaiser, H. F., The Application of Electronic Computers to Factor Analysis. *Educ.*
24 *Psychol. Meas.* **1960**, 20, 141-151.
- 25
26 44. SAR-Caddle. <http://www.cepos-server.com/demoReg/SARcaddle/> (accessed Jan, 2014 -
27 Dec , **2015**)
- 28
29 45. Bax, A.; Davis, D. G., Mlev-17-Based Two-Dimensional Homonuclear Magnetization
30 Transfer Spectroscopy. *J. Magn. Reson.* **1985**, 65, 355-360.
- 31
32 46. Kumar, A.; Ernst, R. R.; Wuthrich, K., A Two-Dimensional Nuclear Overhauser
33 Enhancement (2D Noe) Experiment for the Elucidation of Complete Proton-Proton Cross-
34 Relaxation Networks in Biological Macromolecules. *Biochem. Biophys. Res. Commun.* **1980**, 95,
35 1-6.
- 36
37 47. Palmer, A. G.; Cavanagh, J.; Wright, P. E.; Rance, M., Sensitivity Improvement in
38 Proton-Detected 2-Dimensional Heteronuclear Correlation NMR-Spectroscopy. *J. Magn. Reson.*
39 **1991**, 93, 151-170.
- 40
41 48. Kay, L. E.; Keifer, P.; Saarinen, T., Pure Absorption Gradient Enhanced Heteronuclear
42 Single Quantum Correlation Spectroscopy with Improved Sensitivity. *J. Am. Chem. Soc.* **1992**,
43 114, 10663-10665.
- 44
45 49. Kontaxis, G.; Stonehouse, J.; Laue, E. D.; Keeler, J., The Sensitivity of Experiments
46 Which Use Gradient Pulses for Coherence-Pathway Selection. *J. Magn. Reson.* **1994**, 111, 70-
47 76.
- 48
49 50. Becke, A. D., Density-Functional Thermochemistry .III. The Role of Exact Exchange. *J.*
50 *Chem. Phys.* **1993**, 98, 5648-5652.
- 51
52 51. Lee, C. T.; Yang, W. T.; Parr, R. G., Development of the Colle-Salvetti Correlation-
53 Energy Formula into a Functional of the Electron-Density. *Phys. Rev. B* **1988**, 37, 785-789.
- 54
55 52. Vosko, S. H.; Wilk, L.; Nusair, M., Accurate Spin-Dependent Electron Liquid
56 Correlation Energies for Local Spin-Density Calculations - A Critical Analysis. *Canad. J. Phys.*
57 **1980**, 58, 1200-1211.
- 58
59 53. Stephens, P. J.; Devlin, F. J.; Chabalowski, C. F.; Frisch, M. J., Ab-Initio Calculation of
60 Vibrational Absorption and Circular-Dichroism Spectra Using Density-Functional Force-Fields.
J. Phys. Chem. **1994**, 98, 11623-11627.

- 1
2
3 54. Ditchfield, R.; Hehre, W. J.; Pople, J. A., Self-Consistent Molecular-Orbital Methods .IX.
4 Extended Gaussian-Type Basis for Molecular-Orbital Studies of Organic Molecules. *J. Chem.*
5 *Phys.* **1971**, 54, 724-728.
6
7 55. Hehre, W. J.; Ditchfie.R; Pople, J. A., Self-Consistent Molecular-Orbital Methods .XII.
8 Further Extensions of Gaussian-Type Basis Sets for Use in Molecular-Orbital Studies of
9 Organic-Molecules. *J. Chem. Phys.* **1972**, 56, 2257-2261.
10 56. Hariharan P. C.; Pople, J. A., The Influence of Polarization Functions on Molecular-
11 Orbital Hydrogenation Energies. *Theor. Chim. Acta* **1973**, 28, 213-222.
12 57. Hariharan P. C.; Pople, J. A., Accuracy of AH Equilibrium Geometries by Single
13 Determinant Molecular-Orbital Theory. *Mol. Phys.* **1974**, 27, 209-214.
14 58. Gordon, M. S.; Binkley, J. S.; Pople, J. A.; Pietro, W. J.; Hehre, W. J., Self-Consistent
15 Molecular-Orbital Methods. 22. Small Split-Valence Basis Sets for Second-Row Elements. *J.*
16 *Am. Chem. Soc.* **1982**, 104, 2797-2803.
17 59. Frisch, M. J.; Trucks, G. W.; Schlegel, H. B.; Scuseria, G. E.; Robb, M. A.; Cheeseman,
18 J. R.; Scalmani, G.; Barone, V.; Mennucci, B.; Petersson, M.; Nakatsuji, H.; Caricato, M.; Li, X.;
19 Hratchian, H. P.; Izmaylov, A. F.; Bloino, J.; Zheng, G.; Sonnenberg, J. L.; Hada, M.; Ehara, M.;
20 Toyota, K.; Fukuda, R.; Hasegawa, J.; Ishida, M.; Nakajima, T.; Honda, Y.; Kitao, O.; Nakai, H.;
21 Vreven, T.; Montgomery, J. A. J.; Peralta, J. E.; Ogliaro, F.; Bearpark, M.; Heyd, J. J.; Brothers,
22 E.; Kudin, K. N.; Staroverov, V. N.; Keith, T. A.; Kobayashi, R.; Normand, J.; Raghavachari, K.;
23 Rendell, A.; Burant, J. C.; Iyengar, S. S.; Tomasi, J.; Cossi, M.; Rega, N.; Millam, J. M.; Klene,
24 M.; Knox, J. E.; Cross, J. B.; Bakken, V.; Adamo, C.; Jaramillo, J.; Gomperts, R.; Stratmann, R.
25 E.; Yazyev, O.; Austin, A. J.; Cammi, R.; Pomelli, C.; Ochterski, J. W.; Martin, R. L.;
26 Morokuma, K.; Zakrzewski, V. G.; Voth, G. A.; Salvador, P.; Dannenberg, J. J.; Dapprich, S.;
27 Daniels, A. D.; Farkas, O.; Foresman, J. B.; Ortiz, J. V.; Cioslowski, J.; Fox, D. J. *Gaussian 09*,
28 *Revision C.01*, Revision C.01; Gaussian, Inc.: Wallingford CT, **2010**.
29 60. Tomasi, J.; Mennucci, B.; Cammi, R., Quantum Mechanical Continuum Solvation
30 Models. *Chem. Rev.* **2005**, 105, 2999-3093.
31 61. Haensele, E.; Saleh, N.; Read, C. M.; Banting, L.; Whitley, D. C.; Clark, T., Can
32 Simulations and Modeling Decipher NMR Data for Conformational Equilibria? Arginine-
33 Vasopressin. *J. Chem. Inf. Model.* **2016**, 56, 1798-1807.
34 62. Haensele, E.; Banting, L.; Whitley, D. C.; Clark, T., Conformation and Dynamics of 8-
35 Arg-Vasopressin in Solution. *J. Mol. Model.* **2014**, 20, 2485(17).
36 63. Sikorska, E.; Rodziewicz-Motowidlo, S., Conformational Studies of Vasopressin and
37 Mesotocin Using NMR Spectroscopy and Molecular Modelling Methods. Part I: Studies in
38 Water. *J. Pept. Sci.* **2008**, 14, 76-84.
39 64. Cavanagh, J.; Fairbrother, W. J.; Palmer III, A. G.; Rance, M.; Skelton, N. J., *Protein*
40 *NMR Spectroscopy: Principles and Practice*. 2nd ed.; Elsevier Ltd.: Oxford, **2006**; p 996.
41 65. Grathwohl, C.; Wüthrich, K., NMR Studies of the Rates of Proline Cis–Trans
42 Isomerization in Oligopeptides. *Biopolym.* **1981**, 20, 2623-2633.
43 66. Vitagliano, L.; Berisio, R.; Mastrangelo, A.; Mazzarella, L.; Zagari, A., Preferred Proline
44 Puckerings in Cis and Trans Peptide Groups: Implications for Collagen Stability. *Protein Sci.*
45 **2001**, 10, 2627-2632.
46 67. Smith, S. G.; Goodman, J. M., Assigning Stereochemistry to Single Diastereoisomers by
47 GIAO NMR Calculation: The DP4 Probability. *J. Am. Chem. Soc.* **2010**, 132, 12946-12959.
48
49
50
51
52
53
54
55
56
57
58
59
60

1
2
3
4
5
6
7
8
9
10
11
12
13
14
15
16
17
18
19
20
21
22
23
24
25
26
27
28
29
30
31
32
33
34
35
36
37
38
39
40
41
42
43
44
45
46
47
48
49
50
51
52
53
54
55
56
57
58
59
60

Table of Contents Graphic





ToC Graphic

69x55mm (300 x 300 DPI)

